Effect of Pre-deformation on Decomposition and Spheroidization of M_2C Carbide in High-Speed Steel

XUEFENG ZHOU, WEICHAO ZHANG, ZHIXIA ZHENG, DI LIU, FENG FANG, YIYOU TU, and JIANQING JIANG

One key challenge for tailoring microstructure of high-speed steel (HSS) is to obtain small-sized carbides with a homogeneous distribution. Although diffusion annealing followed by post-deformation offers an opportunity to refine carbides, it requires high annealing temperatures and large strains. In this study, we employ a pre-compression step and examine its role in following carbide decomposition and spheroidization. The result shows that pre-deformation may introduce dislocations into M_2C carbides and hence triggers a significant enhancement of M_2C decomposition into M_6C and MC. Structural defects in M_2C act as potential nucleation sites of new precipitates and activate an alternative decomposition pathway *via* nucleation along dislocations or intersections of stacking faults and dislocations. The decomposition enhancement effect exhibits a dependence on strain and temperature, which may originate from a temperature-mediated balance between dislocation densities and element diffusion rates in M_2C carbides. Compared with post-deformation, pre-deformation facilitates carbide spheroidization and enables smaller carbides as well as higher tempered hardness. This may offer an alternate pathway for carbide refinement in HSS.

https://doi.org/10.1007/s11661-020-05776-3

I. INTRODUCTION

HIGH-SPEED steel (HSS) is a high-carbon multi-component alloy and exhibits superior mechanical properties both at ambient and elevated temperatures such as high hardness, good wear resistance, and reasonable toughness. Its outstanding properties originate from the representative microstructure, *i.e.,* substantial primary carbides embedded in tempered martensite decorated with appreciable nano-sized precipitates. Primary carbides can act as hard particles and determine wear resistance and toughness of HSS. Nevertheless, primary carbides that are products of eutectic solidification are very coarse and heterogeneously distributed along grain boundaries. Large-sized carbides fracture more readily under applied stress and cause a deteriorated fracture toughness. Hence, obtaining small carbides with a homogeneous distribution has been a main challenge for microstructure design of HSS.

Different types of primary carbides may form in HSS, such as M_2C, M_6C, and MC, depending upon chemical compositions and cooling rates.[1] Among them, M_2C is the most predominant type and exists in almost all HSS. Metastable M_2C carbides decompose into a mixture of M_6C and MC carbides at elevated temperatures, facilitating carbide spheroidization and refinement.[2,3] M_2C decomposition and spheroidization occur during the diffusion annealing step in industrial productions of HSS. In most cases, however, diffusion annealing requires a high temperature (1100 °C to 1200 °C) and a prolonged time (1 to 4 hours) for complete carbide decomposition.[3,4] This may induce pronounced coarsening of carbides and consequently a deteriorated toughness of HSS.

In order to overcome shortcomings of diffusion annealing, further heavy plastic deformation such as forging and rolling is usually employed in the industrial production. Post-deformation following diffusion annealing can disperse decomposed carbide mixtures and refine carbide dimensions to some extent. Effective carbide refinement occurs only at very large strains. Nevertheless, large strains cannot be guaranteed in

XUEFENG ZHOU is with the School of Materials Science and Engineering, Southeast University, Nanjing, 211189, P.R. China and also with the Jiangsu Key Laboratory of Advanced Metallic Materials, Southeast University, Nanjing, 211189, P.R. China. Contact e-mail: xuefengzhou@seu.edu.cn WEICHAO ZHANG, ZHIXIA ZHENG, DI LIU, FENG FANG, and YIYOU TU are with the School of Materials Science and Engineering, Southeast University. JIANQING JIANG is with the College of Mechanical and Electronic Engineering, Nanjing Forestry University, Nanjing 210037, P.R. China.

Manuscript submitted September 30, 2019.
Article published online April 24, 2020

many cases. For instance, large-sized carbides remain a big issue in large-section wrought HSS products with limited forging ratios.

Deformation can exert a significant influence on thermodynamics and kinetics of phase transformation. Deformation-induced phase transformation, such as deformation-induced martensite transformation (DIMT)[5] and ferrite transformation (DIFT),[6] has been observed in various alloy systems. Transformation-induced plasticity (TRIP) that derives from DIMT has been applied to enhance the ductility of medium-Mn steels and quench and partitioning steels. The TRIP effect is closely correlated with austenite stability, which depends on chemical compositions,[7] grain sizes of austenite,[8] as well as external deformation parameters,[9–11] including temperature, strain, stress state, *etc*. Many researchers have studied the kinetics of DIMT under various conditions. For example, Olson and Cohen found that shear band intersections act as nucleation sites of martensite and proposed an empirical kinetics equation between the volume fraction of transformed martensite and plastic strain.[12] Iwamoto,[13] Stringfellow,[14] and Shin[15] also tried to generalize the Olson and Cohen model and incorporated other factors into the model such as stress state and austenite stability.

Inspired by DIFT and DIMT, we employed a pre-compression step prior to carbide decomposition and firstly observed a decrease of M_2C decomposition temperature, which is referred to as deformation-induced carbide transformation (DICT).[16] In this study, we systematically investigate the effect of pre-strain and temperature on carbide decomposition and spheroidization, and explore an alternate pathway for carbide refinement by tailoring M_2C decomposition through pre-deformation. Compared with post-compression, pre-compression enhances significantly M_2C decomposition and following carbide spheroidization, enabling smaller-sized carbides and higher tempered hardness. The enhancement of carbide decomposition depends on strain and temperature, originating from a balance between dislocation densities and element diffusion rates in carbides. The new method developed in this work, *i.e*., pre-compression followed by carbide decomposition and spheroidization, requires lower temperatures and smaller strains to completely decompose and disperse carbides, which may offer an opportunity to address the issue of conventional processing route of HSS.

II. EXPERIMENTAL

The material used in this study was AISI M2 HSS with a composition of $C_{0.82}W_{5.80}Mo_{4.69}Cr_{4.04}V_{1.90}Si_{0.31}Mn_{0.33}Fe_{bal}$ (wt pct). The deoxidized molten steel was cast in an iron mold with a diameter of 120 mm. Cylindrical samples of 6 mm in diameter and 12 mm in height were sliced from annealed ingots, and then compressed with a ratio of 20, 40, and 50 pct at ambient temperature using a CMT 100-kN testing machine. The equivalent strains are about 0.2, 0.5, and 0.7, respectively. The specimens used in following examination were sliced from the center of compressed samples.

Uncompressed and pre-compressed samples were heated at 1050 °C for 30 minutes to decompose M_2C carbides. In order to elucidate factors affecting carbide decomposition, pre-compressed samples were subjected to a recrystallization pre-treatment performed at 750 °C for 6 hours, followed by diffusion annealing at 1100 °C for 30 minutes. Carbide powders extracted from uncompressed and pre-compressed samples were heated at 1100 °C for 120 minutes in a vacuum furnace. Pre-compressed samples were also heated for 30 minutes at 1000 °C, 1050 °C, 1100 °C, and 1150 °C, respectively, to examine the temperature dependence of carbide decomposition.

Two different processing routes were employed to process HSS. One was the conventional processing route wherein carbide decomposition precedes spheroidization and compression, which hereinafter is referred to as post-compression. The other was a novel processing route explored in this work wherein pre-compression was conducted prior to carbide decomposition and spheroidization. Post- and pre-compression strain was set as 0.5. Carbide decomposition was performed at 1050 °C for 5 hours while carbide spheroidization was carried out at 1160 °C for 20, 30, 60, and 90 minutes, respectively. The hardness of samples was measured after austenitizing at 1200 °C for 3 minutes, followed by oil quenching and double tempering at 560 °C for 90 minutes.

Two- and three-dimensional morphologies of carbides were observed by FEI Sirion-400 scanning electron microscope (SEM) under the secondary electron mode after etching with 4 pct nital and an etchant of 5 mL HF + 100 mL H_2O_2, respectively. The ImageJ software was employed to measure the volume fraction of total carbides and specified carbide types. M_2C, M_6C, and MC carbides can be identified as dark gray, light gray, and dark phases in a backscattered electron image due to different chemical compositions, respectively.[17] The relative fraction of specified carbide type was calculated by its volume fraction divided by that of total carbides.

The microstructural evolution and decomposition process of primary carbides were examined by transmission electron microscope (TEM) and X-ray diffraction (XRD). Thin foils were prepared by mechanical polishing and twin-jet electropolishing, and then examined by Tecnai G2 TEM, operating at an accelerating voltage of 160 kV. XRD was carried out in the range of 30 to 80 deg glancing angles at a scan speed of 0.2 deg/min, using a Bruker D8 diffractometer with Cu Kα radiation, operating at 40 kV and 30 mA. The specimens for XRD were carbide powders extracted from ingots, which was performed using electrolysis operating at 0 °C with a current of 0.5 A. The electrolyte contained 7 g citric acid, 20 mL hydrochloric acid, and 250 mL methanol. Carbide powders were collected from the electrolyzed ingots using supersonic vibration and centrifugation in the deionized water, followed by further drying at 60 °C and grinding in a corundum bowl.

III. RESULTS

A. *Microstructural Evolution During Pre-compression*

Figure 1 shows three-dimensional morphologies of primary carbides in M2 ingots. The as-cast structure consists of plate-like carbide networks heterogeneously distributed in interdendritic regions. Plate-like carbides are identified as the M_2C type with a hexagonal close-packed structure.[17] After compression, M_2C carbide plates are mechanically crushed into smaller fragments and their dimensions decrease with increasing strain. However, M_2C carbides exhibit a quite limited plastic deformability at ambient temperature. They present few morphological characteristics of plastic deformation and retain the flat plate shape as illustrated in Figure 1(b).

Further TEM examination provides more details about the substructure of ferrite grains and M_2C carbides (Figures 2 and 3). Ferrite grains are decorated with high densely dispersive secondary carbides and exhibit a very low density of dislocations before compression. Intrinsic stacking faults are occasionally observed in M_2C carbides. Pre-compression produces a high density of dislocations in ferrite especially around secondary precipitates, forming dislocation cells and walls as shown in Figure 2(b). Although M_2C carbides present few deformation characteristics in appearance, pre-compression creates dislocations in M_2C, which intersect stacking faults. It seems that pre-compression may also induce stacking faults in carbides since stacking faults are more frequently identified after compression. An increasing pre-strain enables a higher density of dislocations in both ferrite and M_2C. Compared with ferrite grains, M_2C carbides display lower dislocation densities at a given strain.

B. *Evolution of M_2C Decomposition with Pre-strain*

Figure 4 illustrates the microstructure of M2 ingots after heating at 1050 °C for 30 minutes. Metastable M_2C carbides decompose into a mixture of M_6C and MC carbides. However, there still exists a large amount of residual M_2C carbides, which display a relative volume fraction of ~ 55 pct in total carbides of the uncompressed ingot. By contrast, pre-compression significantly accelerates M_2C decomposition and enables fewer residual M_2C carbides. This result strongly demonstrates that pre-compression may facilitate M_2C decomposition.

Quantitative statistics and XRD results also evidence this point (Figures 5 and 6). An increase of pre-strain enables stronger diffraction intensities of M_6C and MC products, accompanied by lower intensities of parent M_2C carbides. The relative volume fraction of residual M_2C in total carbides drops to only ~ 10 pct in the ingot with a pre-strain of 0.7. These findings suggest that a larger pre-strain may yield a higher decomposition rate. M_6C and MC exhibit quite different growing rates during decomposition. The volume fraction of M_6C carbides increases more rapidly with increasing strain, suggesting a higher growth rate compared to the MC counterpart. We also note that some voids or cracks are created at the carbide/matrix interface with increasing strain due to the limited deformation compatibility between the matrix and carbides at ambient temperature. It is expected that warm deformation could improve the flowability of metal matrix and enable the elimination of voids while retain the enhancement effect of carbide decomposition.

In addition, pre-compression modifies the transformation pathway of M_2C carbides as shown in Figure 4. In the uncompressed ingot, M_6C and MC products are created at the M_2C/matrix interface, whereas residual M_2C is observed in the interiors of carbide plates. This implies that M_2C carbides are decomposed in a common interface-nucleation mode.[18] By contrast, pre-compression enables substantial precipitation of M_6C and MC both in the interiors of M_2C plates and at the M_2C/matrix interface. A larger pre-strain produces more precipitates in carbide interiors compared to those formed at the interface. This result suggests that pre-compression may induce an evolution of M_2C decomposition pathway from an interface-nucleation mode alone to a mixed mode of interface- and interior-nucleation.

C. *Evolution of M_2C Decomposition with Temperature*

Figure 7 shows quantitative statistics of decomposed microstructures in the uncompressed and pre-compressed M2 ingots. An increase of temperature

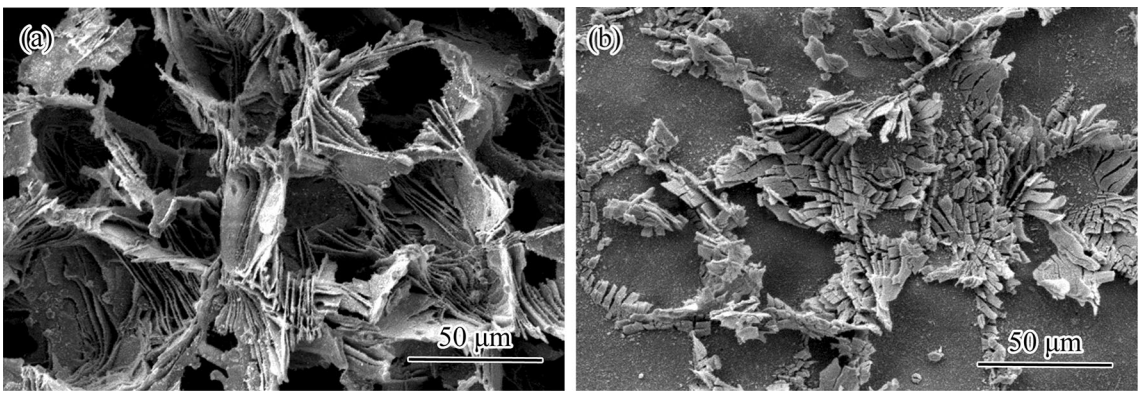

Fig. 1—Three-dimensional morphologies of M_2C primary carbides in M2 ingots with a pre-strain of (*a*) 0 and (*b*) 0.5.

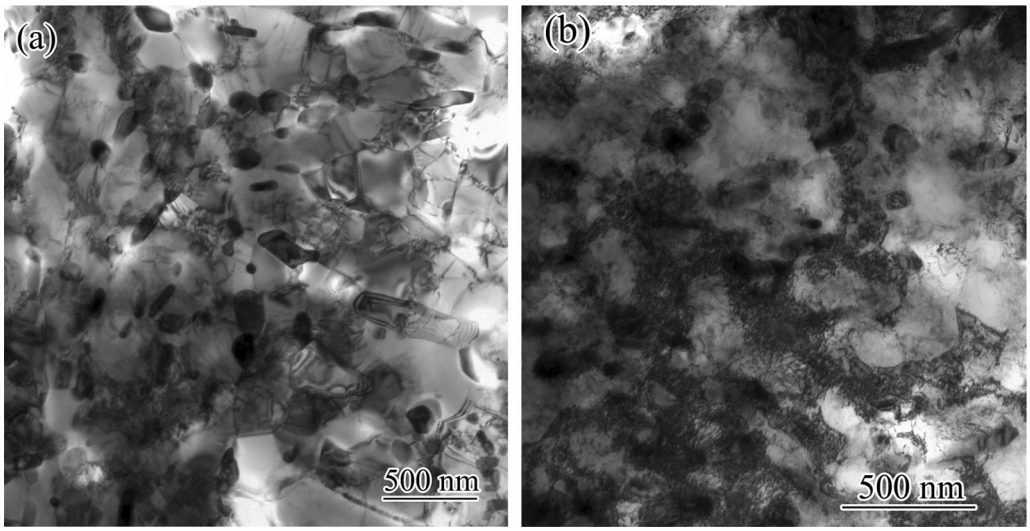

Fig. 2—Microstructure of ferrite grains in M2 ingots with a pre-strain of (*a*) 0 and (*b*) 0.5.

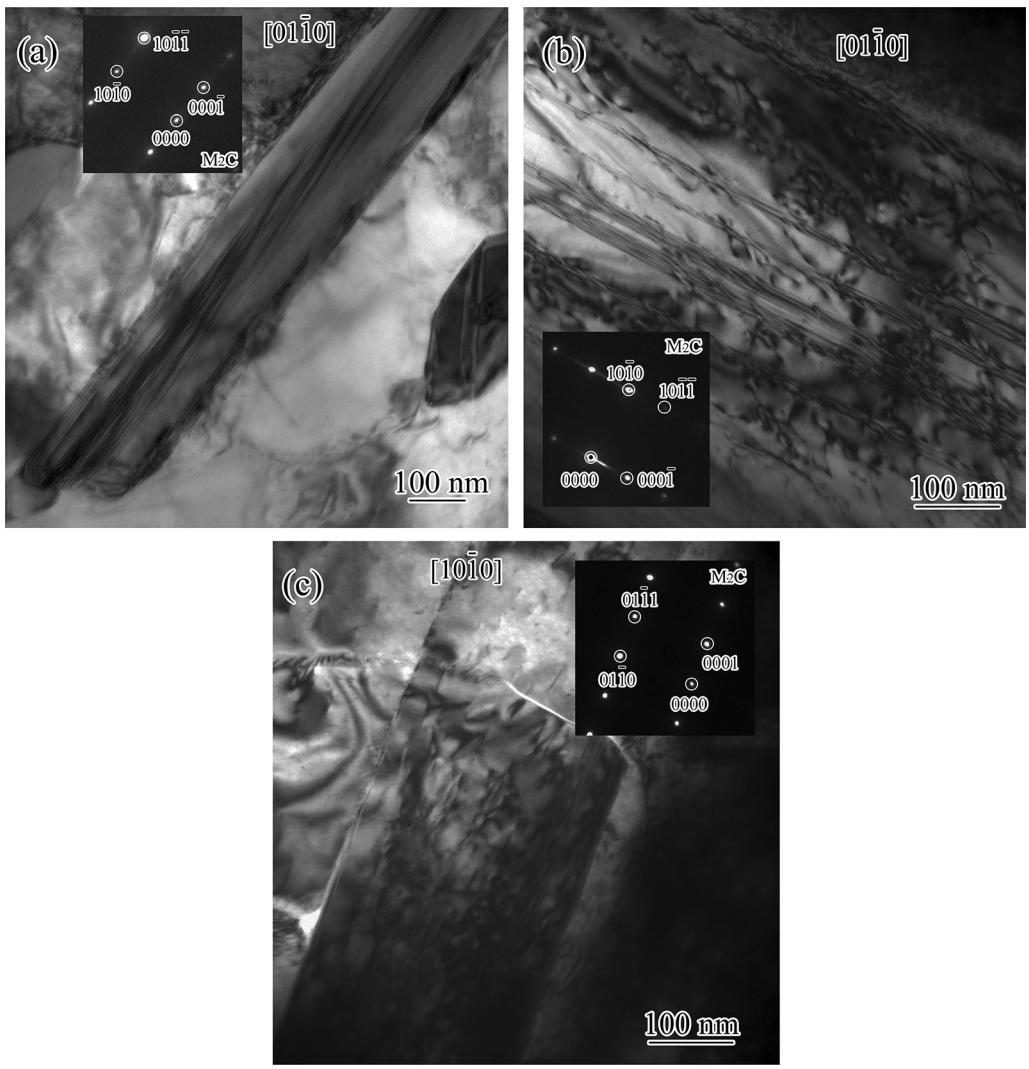

Fig. 3—Bright-field images of M_2C carbides in M2 ingots with a pre-strain of (*a*) 0, (*b*) 0.2, and (*c*) 0.5, which are viewed from the $[01\bar{1}0]$, $[0\bar{1}\bar{1}0]$, and $[10\bar{1}0]$ zone axis, respectively.

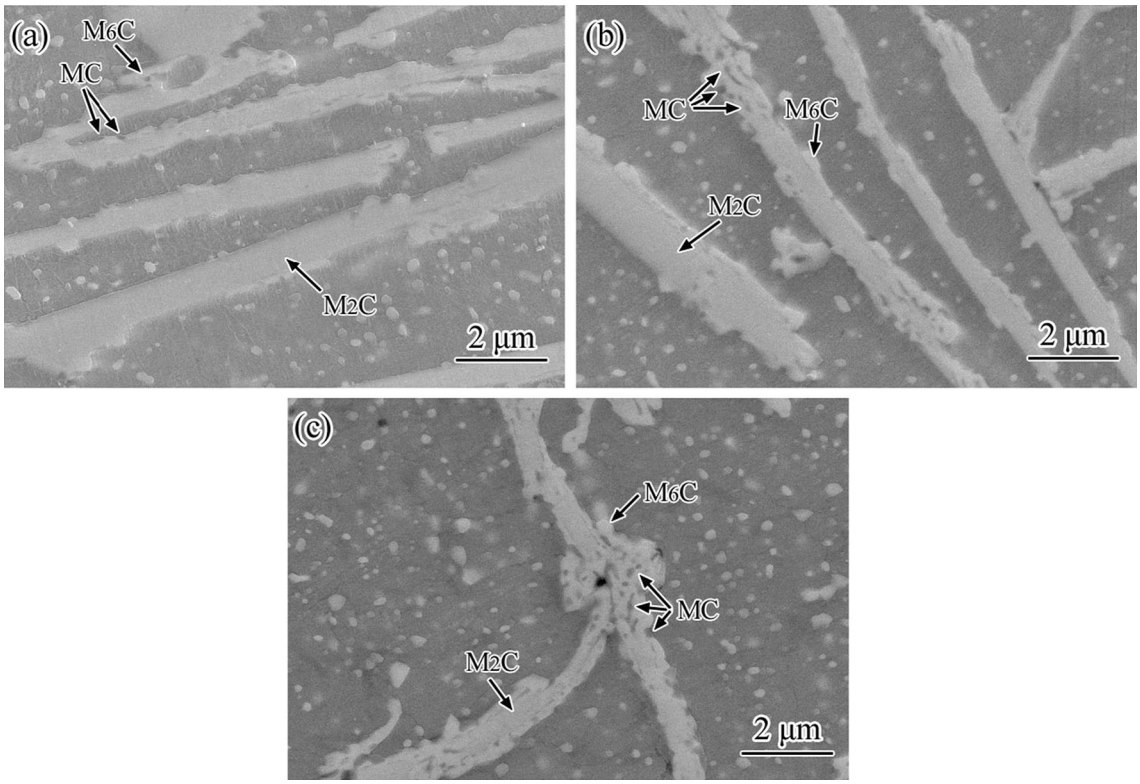

Fig. 4—Microstructure of M2 ingots with a pre-strain of (*a*) 0, (*b*) 0.2, and (*c*) 0.5 followed by heating at 1050 °C for 30 min.

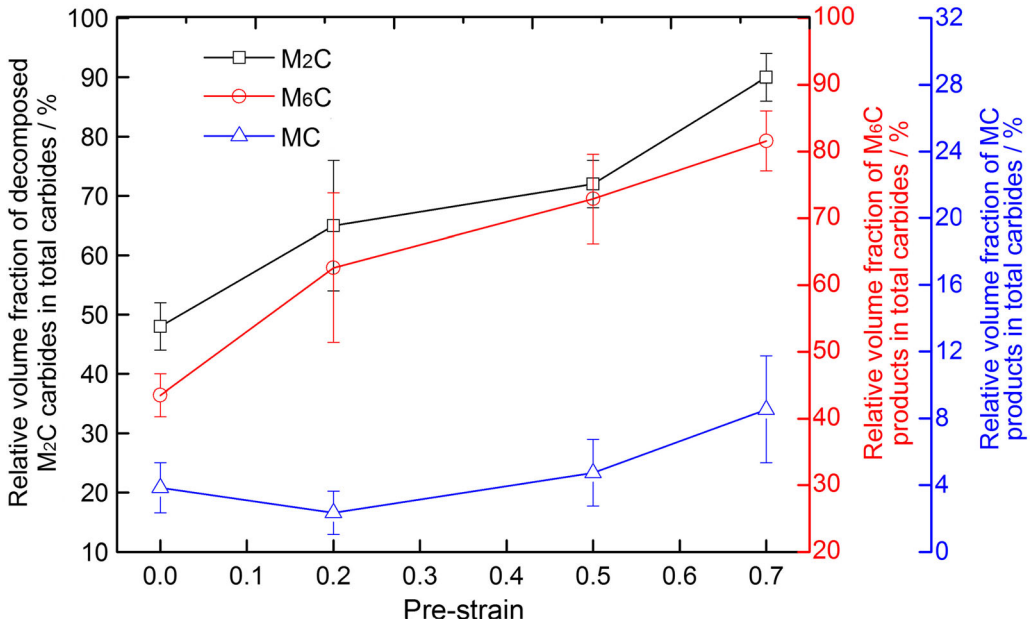

Fig. 5—Relative volume fraction of decomposed M_2C carbides, M_6C and MC products in total carbides in M2 ingots with different pre-strains followed by heating at 1050 °C for 30 min.

accelerates significantly M_2C decomposition and enhances the precipitation of decomposition products in both ingots. Pre-compression produces a much lower fraction of residual M_2C and a higher number density of new products at a given temperature. M_2C carbides almost decompose completely in the pre-compressed ingot after heating at 1150 °C for 30 minutes, whereas residual M_2C with a relative volume fraction

of ~ 9 pct in total carbides still exists in the uncompressed counterpart. This result further evidences the acceleration of M_2C decomposition by pre-compression.

Although an elevated temperature causes higher decomposition rates in both ingots, the compression-enhanced decomposition effect, defined by the relative volume fraction of decomposed M_2C in the compressed ingot subtracted by that in the uncompressed one, does not increase linearly with the temperature (Figure 8). It is found that either a higher or lower temperature is unfavorable for the increment of M_2C decomposition fraction despite the relatively large error bars, which may arise from the chemical and strain in homogeneity of various carbides. The decomposition enhancement effect seemingly displays a temperature dependence and the optimal temperature is around 1050 °C.

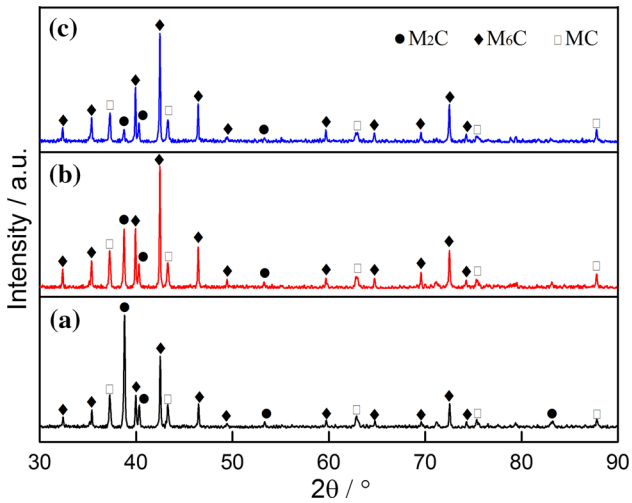

Fig. 6—XRD profiles of carbide powders extracted from M2 ingots with a pre-strain of (*a*) 0, (*b*) 0.5, and (*c*) 0.7 followed by heating at 1050 °C for 30 min.

D. *Role of Compression-Induced Defects in M_2C Decomposition*

It can be rationalized that the enhancement of M_2C decomposition should be a consequence of compression-induced defects in either the matrix or M_2C carbides. In order to elucidate different factors underlying carbide decomposition, recrystallization pre-treatment and carbide powder extraction were conducted, respectively. The recrystallization pre-treatment, *i.e.,* heating at 750 °C for 6 hours, is conducted on the pre-compressed ingot and followed by diffusion annealing at 1100 °C for 30 minutes, the aim of which is to reduce dislocation densities in ferrite grains and unveil its role in M_2C decomposition. Carbide powders were extracted from the compressed ingots and then heated in vacuum at 1100 °C for 120 minutes in order to examine the effect of structural defects in carbides on decomposition.

Figure 9 shows the microstructure of ferrite grains and M_2C carbides in M2 ingot with a pre-strain of 0.5

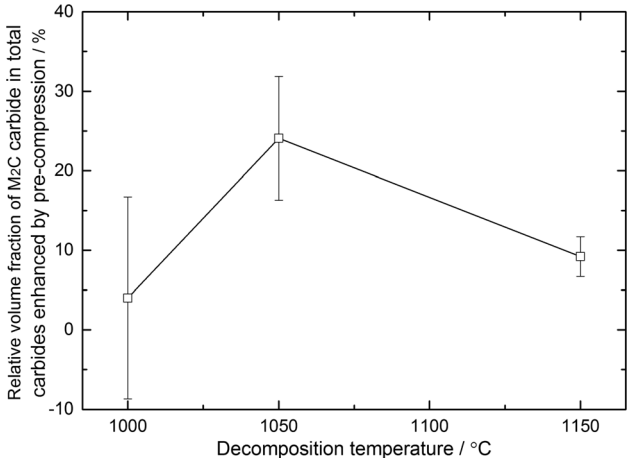

Fig. 8—Compression-enhanced M_2C decomposition fraction at different decomposition temperatures.

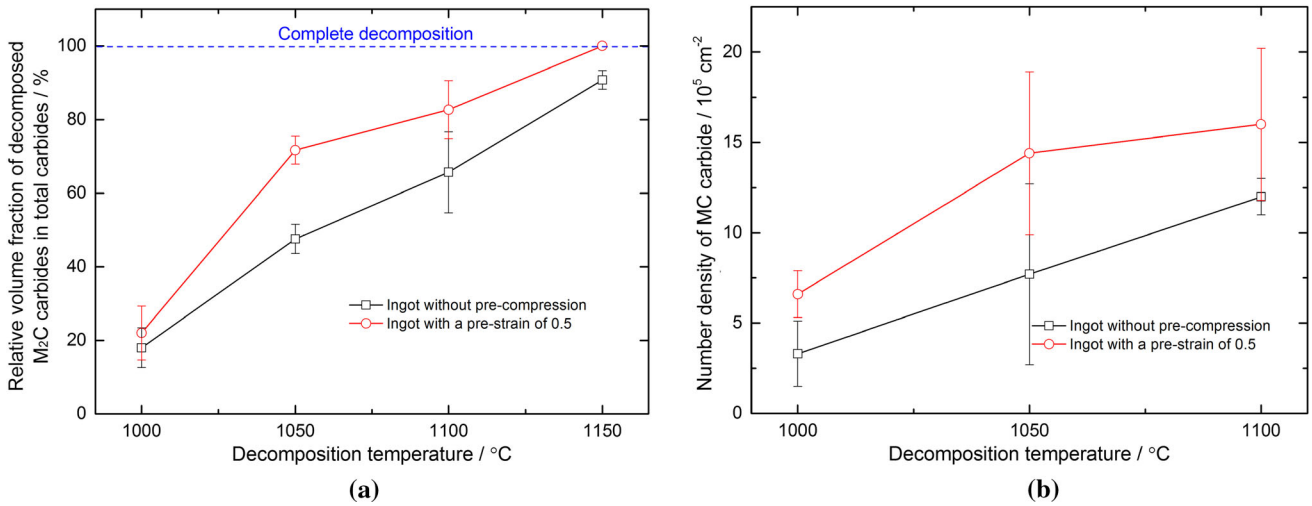

Fig. 7—Quantitative statistics of (*a*) relative volume fraction of decomposed M_2C carbides in total carbides and (*b*) number density of MC products in uncompressed and pre-compressed ingots with increasing temperature.

followed by recrystallization pre-treatment. The pre-treatment enables a significant decrease of dislocation densities and produces fine recrystallized ferrite grains. These recrystallized grains exhibit low dislocation densities that are comparable with ferrite grains in the uncompressed ingot. Pre-treatment also induces a lower density of dislocations in M_2C carbides. Despite partial annihilation of dislocations after the pre-treatment, there still exists a certain number of dislocation lines as well as stacking faults inside M_2C carbides as shown in Figure 9(b).

Figure 10 illustrates the microstructure of M2 ingots after heating at 1100 °C for 30 minutes. A large portion of residual M_2C carbides still exists in the uncompressed ingot, whereas M_2C carbides almost decompose completely in the pre-compressed ingot. Although the recrystallization pre-treatment produces ferrite grains with low dislocation densities comparable to those without compression, M_2C carbides in the recrystallized ingot still decompose much faster than those in the uncompressed ingot. Only a very small amount of retained M_2C can be observed as shown in Figure 10(c). It can be rationalized that the higher M_2C decomposition rate in this case should be a consequence of residual structural defects in carbides. Compression-induced dislocations in M_2C are more active in the carbide decomposition compared to dislocations in ferrite grains.

Figure 11 illustrates XRD profiles of carbide powders after heating at 1100 °C for 120 minutes. Compared with carbide powders collected from the uncompressed ingot, M_2C carbides extracted from the pre-compressed ingot display much lower diffraction intensities. This result further evidences that structural defects in carbides trigger higher decomposition rates of M_2C carbides.

It should be pointed out that the decomposition products of carbide powders exhibit quite different compositions compared to those of bulk samples. MC carbides in the decomposed carbide powders display much stronger diffraction peaks than M_6C products, which is contrary to the case of ingots wherein M_6C carbides are the predominant products and present stronger diffraction intensities as shown in Figure 6. This difference may originate from the change of decomposition environment correlated with essential elements for decomposition products. For M_2C decomposition in bulk samples, M_2C parent carbides may provide W or Mo for M_6C and V for MC, whereas the matrix mainly offers Fe for M_6C.[19] After the removal of matrix, however, M_2C carbide powders cannot guarantee sufficient Fe concentrations that are necessary for M_6C. The lack of Fe hence produces a smaller portion of M_6C products in the case of carbide powders after decomposition.

E. *Nucleation Mode of M_2C Decomposition*

The above results illustrate that pre-compression may modify M_2C decomposition pathway. Further TEM examination sheds more light on the underlying mechanism (Figure 12). In the uncompressed ingot, M_6C is nucleated at the matrix/M_2C interface while MC is formed at either the M_6C/M_2C or matrix/M_2C interface, demonstrating an interface-nucleation mode of M_2C decomposition that is active in most cases.[18] Interface-nucleated precipitates are also observed in the pre-compressed ingot with a strain of 0.2 (Figure 12(b)). Meanwhile, a few nano-sized precipitates are formed on dislocations inside carbides. A larger pre-strain produces more precipitates in carbide interiors (Figures 12(c) and (d)). These granular or disc-like

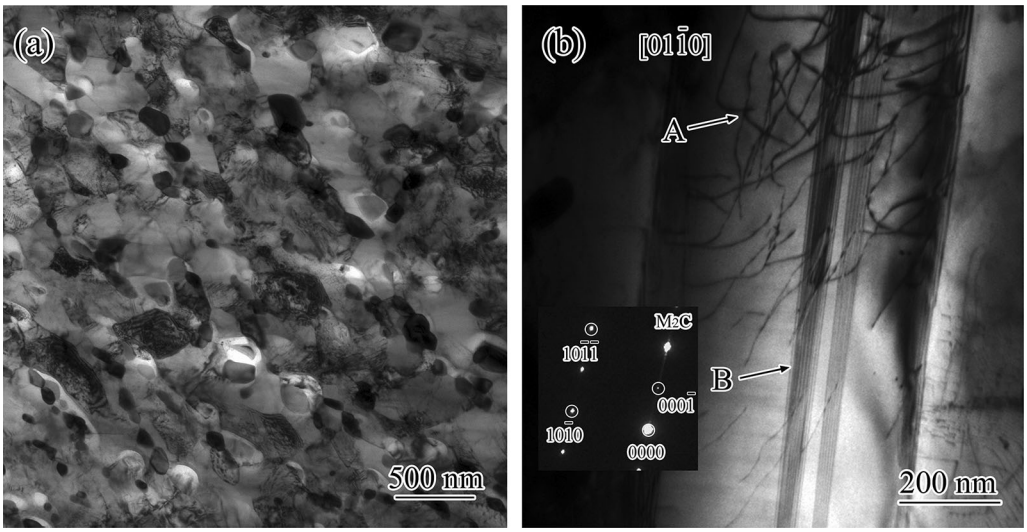

Fig. 9—Microstructure of (*a*) ferrite grains and (*b*) M_2C carbides in the pre-compressed ingot with a strain of 0.5 followed by recrystallization pre-treatment at 750 °C for 6 h. The arrows A and B in Figure (*b*), viewed from the $[01\bar{1}0]$ zone axis, denote the residual dislocations and stacking faults in carbides, respectively.

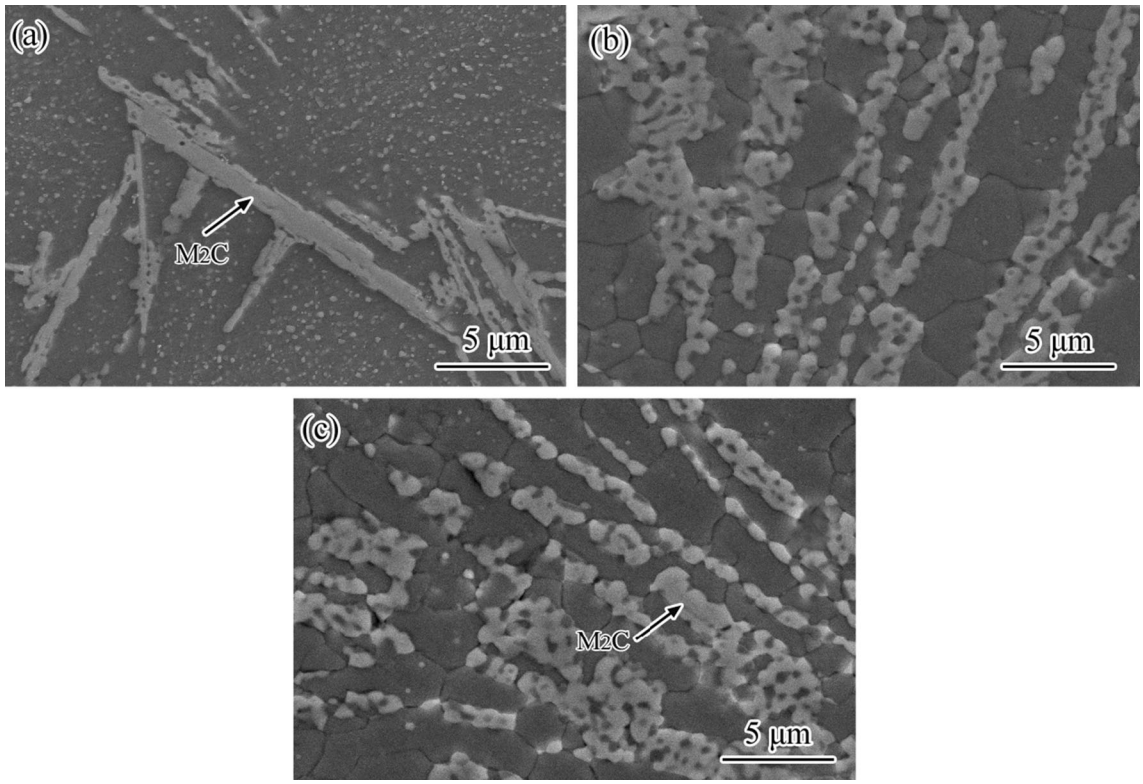

Fig. 10—Microstructure of M2 ingots with a pre-strain of (*a*) 0, (*b*) 0.5 without pre-treatment, and (*c*) 0.5 with pre-treatment at 750 °C for 6 h, followed by heating at 1100 °C for 30 min.

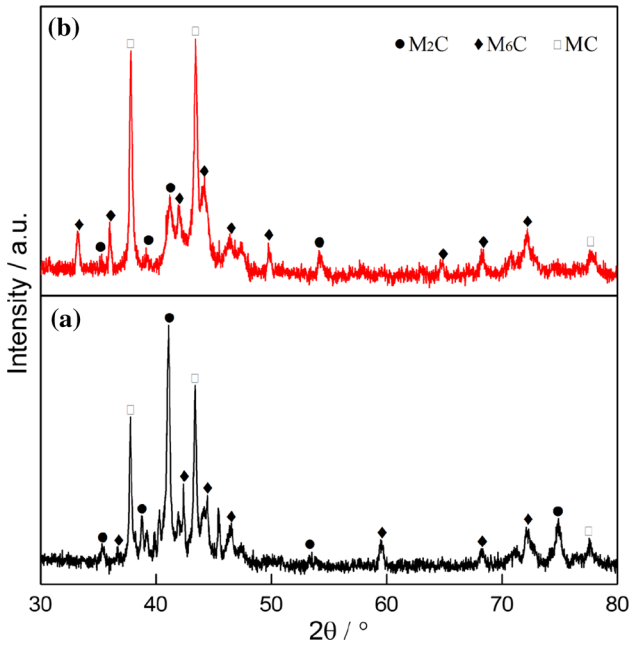

Fig. 11—XRD profiles of carbide powders extracted from M2 ingots with a pre-strain of (*a*) 0 and (*b*) 0.5, and then heated in vacuum at 1100 °C for 120 min.

precipitates, identified as either M_6C or MC,[16] are nucleated either along dislocation lines or at the intersections of stacking faults and dislocations. This result strongly evidences that compression-induced structural defects can act as heterogeneous nucleation sites of new precipitates and activate a novel dislocation-nucleation manner. The higher number density of precipitates in carbide interiors with increasing strain suggests that pre-strain may reinforce the dislocation-nucleation mode compared to the common interface-nucleation manner.

Figure 13 shows the microstructure of M_2C carbides in pre-compressed ingots with a strain of 0.5 after decomposition at various temperatures. After heating at 1000 °C, there exist a certain number of residual dislocations, which are occasionally decorated with a small amount of nano-sized precipitates. An increase in decomposition temperature induces lower dislocation densities. However, a higher number density of new precipitates is observed on residual structural defects (Figure 13(b)). When decomposition temperature reaches 1100 °C, few dislocation lines are retained in carbides and the precipitate number density drops sharply. New precipitates are mainly formed at the matrix/M_2C interface, suggesting a predominant interface-nucleation mode in this case. Despite low number of densities, the precipitates exhibit larger dimensions due to high growing rates at the elevated decomposition temperature. It is reasonably inferred that the effect of pre-compression on M_2C decomposition may be correlated with both nucleation and growth process of new precipitates, which is a synergetic consequence of temperature-dependent dislocation density and element diffusion.

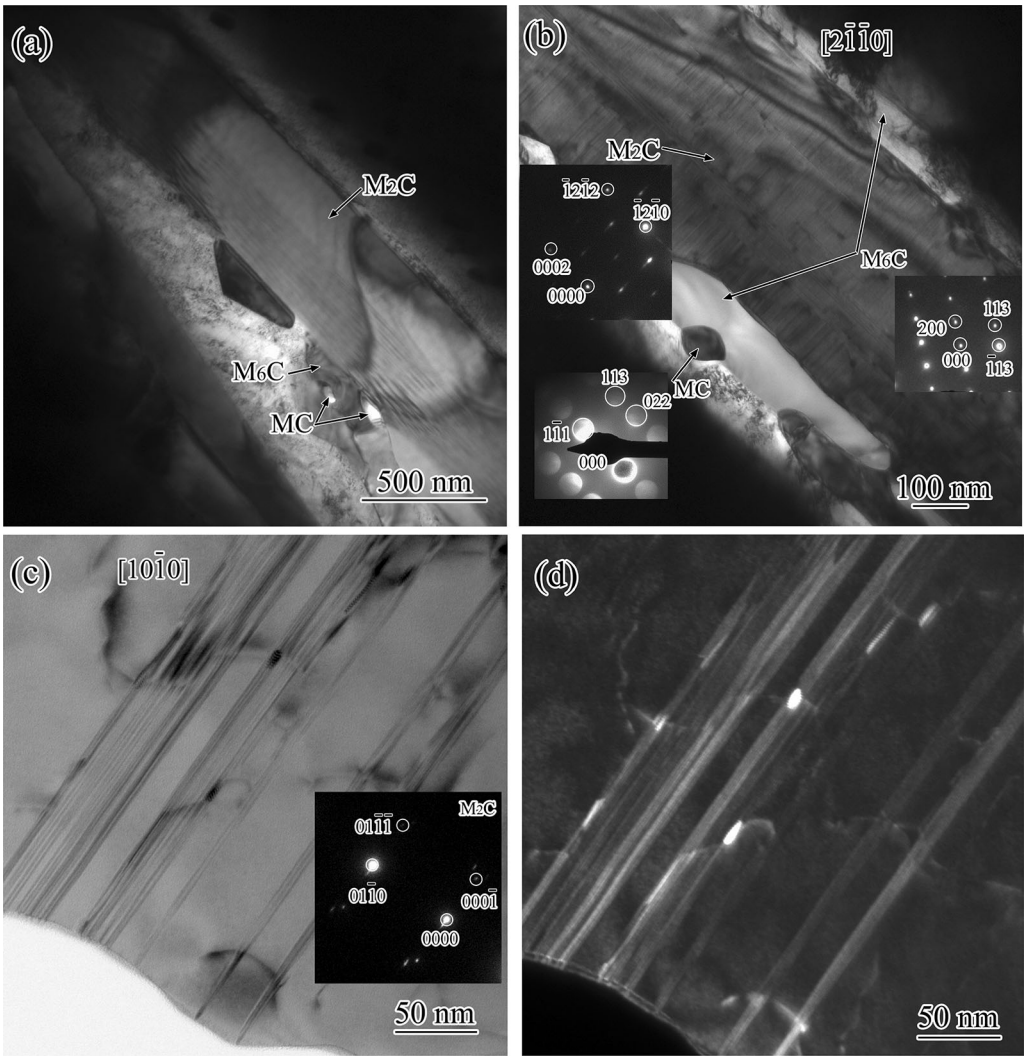

Fig. 12—Nucleation of decomposition products in M2 ingots with a pre-strain of (*a*) 0, (*b*) 0.2, and (*c*, *d*) 0.5. (c) and (d) show the bright-field and corresponding dark-field images of precipitates nucleated along structural defects in carbides. (b) and (c) are viewed from the $[2\bar{1}\bar{1}0]$ and $[10\bar{1}0]$ zone axis, respectively.

F. *Microstructural Homogeneity and Mechanical Properties*

Spheroidization treatment is conducted following carbide decomposition at the optimal temperature (1050 °C). Figures 14 and 15 illustrate spheroidized microstructures of M2 ingots for different conditions and corresponding quantitative statistics, respectively. It is found that both pre- and post-compression can enhance carbide spheroidization and enable smaller carbides. Compared with post-compression, pre-compression produces carbide particles with smaller radiuses and aspect ratios. Prolonging spheroidization time induces a gradual coarsening of carbide particles. Nevertheless, the pre-compressed ingot always exhibits smaller-sized carbides compared to the post-compressed counterpart. This suggests that pre-compression may significantly enhance carbide spheroidization, offering an alternate pathway of carbide refinement.

Figure 16 shows the quenching-tempering microstructure of M2 ingots for different conditions. Austenitization enables partial dissolution of primary carbides and hence a smaller portion of residual carbide networks. Compared with post-compression, pre-compression promotes carbide dissolution and produces a lower volume fraction of undissolved carbides. This occurs due to higher dissolution rates of smaller carbides compared to large-sized particles, which induces increasing concentrations of carbon and carbide-forming elements in martensite. The higher supersaturation may produce more coherent nano-precipitates during subsequent tempering and favor an enhancement of tempered hardness. As illustrated in Figure 17, pre-compression with a strain of 0.5

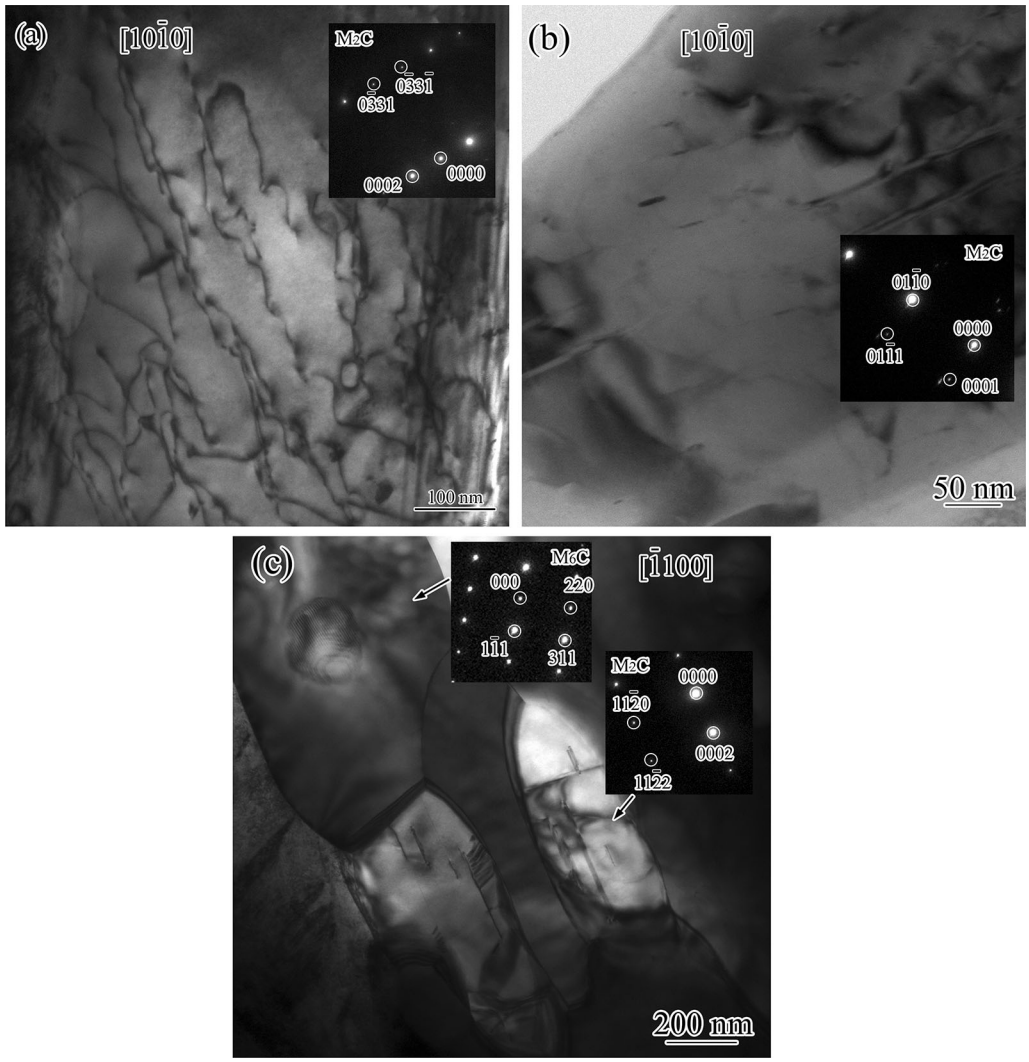

Fig. 13—Bright-field images of precipitates in the pre-compressed ingot with a strain of 0.5 followed by heating for 30 min at (*a*) 1000 °C, (*b*) 1050 °C, and (*c*) 1100 °C, which are viewed from the $[10\bar{1}0]$, $[10\bar{1}0]$, and $[\bar{1}100]$ zone axis, respectively.

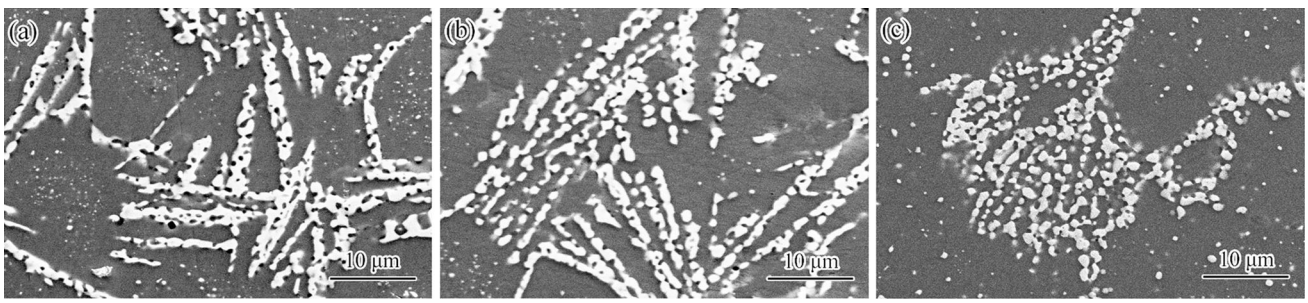

Fig. 14—Microstructure of (*a*) uncompressed ingot, (*b*) post-compressed ingot with a strain of 0.5, and (*c*) pre-compressed ingot with a strain of 0.5, followed by carbide decomposition at 1050 °C for 5 h and spheroidization treatment at 1160 °C for 30 min.

enables an increase of tempered hardness by almost 1.5 HRC compared to the post-compression counterpart. Prolonging spheroidization time causes a slight decrease of tempered hardness, which originates from carbide coarsening and resultantly a lower supersaturation after quenching.

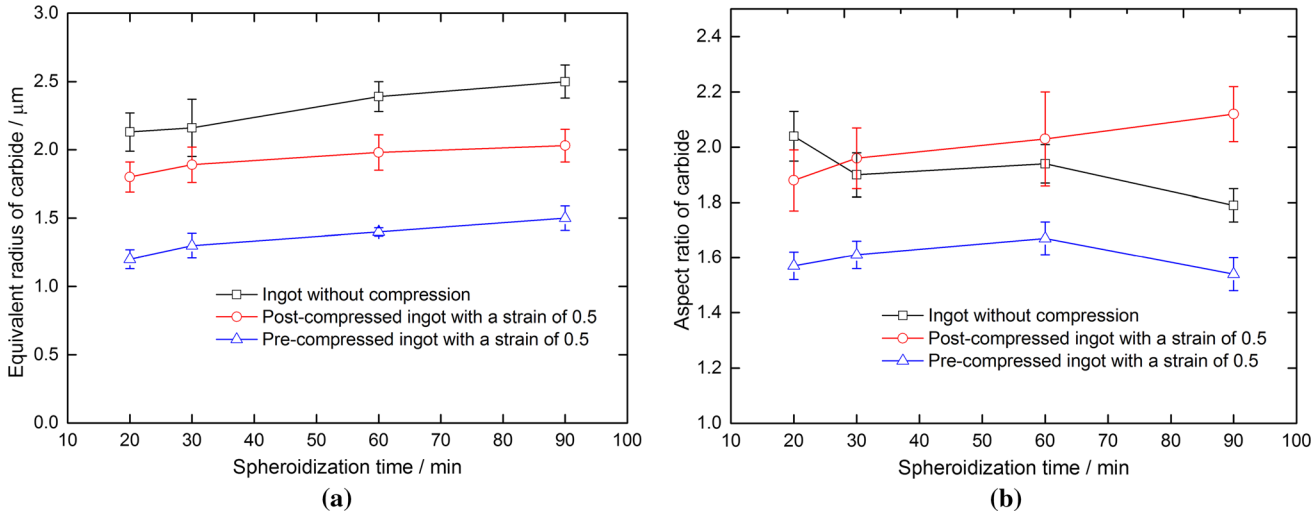

Fig. 15—(*a*) Equivalent radius and (*b*) aspect ratio of carbides in M2 ingots after carbide decomposition at 1050 °C for 5 h followed by spheroidization treatment at 1160 °C for 30 min.

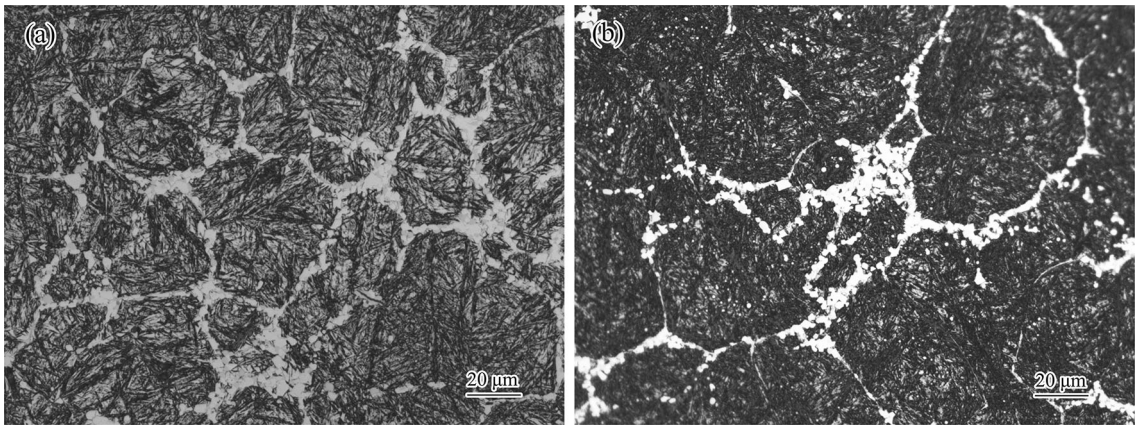

Fig. 16—Tempered microstructure of (*a*) post-compressed ingot and (*b*) pre-compressed ingot both with a strain of 0.5.

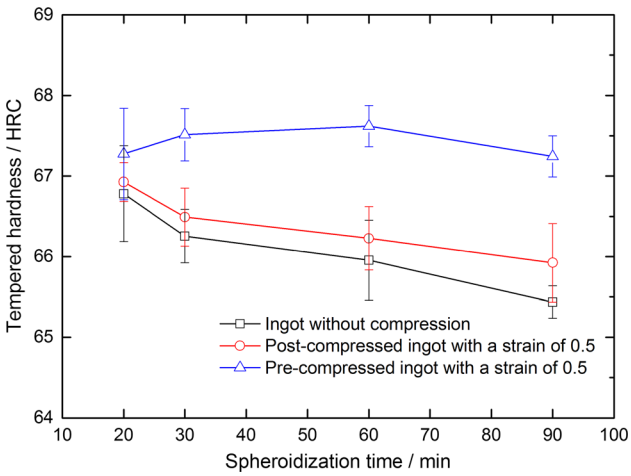

Fig. 17—Tempered hardness of M2 ingots for different conditions.

IV. DISCUSSION

A. *Underlying Mechanism of Enhanced M_2C Decomposition Rates*

HCP-M_2C carbides can hardly undergo plastic deformation at ambient temperature and display few distorted characteristics in shape. The limited deformability of transition metal carbides originates from a low dislocation mobility due to a high Peierls stress.[20] Although M_2C carbides present few deformation characteristics in appearance, pre-compression may introduce dislocations into carbides, implying the room-temperature deformation of M_2C *via* dislocation slip. Similar deformation mechanisms have also been identified in other transition metal carbides with a HCP structure such as Ta_2C and WC.[21,22]

Structural defects in M_2C play a predominant role in the enhancement of M_2C decomposition. These defects can act as potential nucleation sites and produce

substantial M_6C and MC precipitates formed in carbide interiors. In addition, they can enhance diffusion rates of substitutional elements inside carbides and therefore enable higher precipitate growing rates. It can be rationalized that a synergetic enhancement of precipitate nucleation and growth is responsible for higher M_2C decomposition rates. With increasing strain, more dislocations are created in carbides and enable higher precipitate nucleation and growth rates, which significantly accelerate M_2C decomposition.

Heterogeneous precipitation along structural defects, such as dislocations, low-angle boundaries, and stacking faults, was reported in various systems.[23,24] These defects have strong attractive interactions with solutes, which consequently induces element segregation. Both experimental observation and theoretical calculation have evidenced this point.[25,26] The elastic field around defects in M_2C carbides favors precipitate nucleation due to the possibility of releasing the excess free energy and reducing the total interface-free energy. Hence, compression-induced M_6C and MC precipitates along structural defects may be a result of sufficient element segregation in conjunction with local elastic distortion.

Dislocations in the matrix also affect M_2C decomposition since the decomposition occurs in an interface-nucleation manner. These defects can enhance element diffusion rates in the matrix and therefore promote the formation of decomposition products at the matrix/M_2C interface. Once a thin product layer is formed at the interface, however, dislocations in the matrix have little impact on the following decomposition process considering a high diffusion activation energy of substitutional elements inside carbides.[2] It can be rationalized that dislocations in the matrix may be only active in the initial stage of M_2C decomposition.

B. *Correlation Between Temperature and M_2C Decomposition*

M_2C decomposition is a typical diffusional phase transformation, including an evolution of both crystal structure and chemical composition. Fe and W or Mo diffuse into M_6C, whereas *V* is segregated into MC.[18] Hence, element diffusion inside carbides dominate the decomposition.[2] An increase of temperature accelerates the element diffusion and hence enables higher decomposition rates of M_2C carbides.

Dislocations in M_2C carbides, acting as potential nucleation sites and rapid diffusion channels, can facilitate both precipitate nucleation and growth. Hence, the enhancement of M_2C decomposition depends on dislocation densities together with element diffusion rates in carbides. A lower decomposition temperature ensures higher dislocation densities, whereas weakens the element diffusion capability, which may suppress precipitate nucleation and growth. Although an increase of decomposition temperature enables higher element diffusion rates and precipitate growth rates, it causes lower residual dislocation densities and fewer potential nucleation sites of new precipitates. In the case of pre-compression, M_2C decomposition is mediated by the balance between dislocation densities and element diffusion rates, both of which depend on decomposition temperature. This is responsible for the temperature dependence of M_2C decomposition enhancement induced by pre-compression. The optimal decomposition temperature in the present work is around 1050 °C probably due to a good combination of retained dislocation densities and element diffusion rates.

C. *Decomposition Pathway of M_2C Carbide*

The interface-nucleation mode dominates M_2C decomposition in most cases. M_6C enriched in Fe and W or Mo is firstly formed at the matrix/M_2C interface, followed by nucleation of *V*-rich MC at the matrix/M_2C or M_6C/M_2C interface.[18] The aforementioned decomposition pathway arises from chemical compositions of new precipitates.[19] The parent M_2C carbides provide almost all elements required for new precipitates except Fe. Instead, the matrix may offer abundant Fe for M_6C precipitates, which induces M_6C nucleation at the matrix/M_2C interface. M_6C precipitation causes V segregation and hence facilitates the following nucleation of MC precipitates at the M_6C/M_2C interface.

Compression-induced defects in carbides activate an alternative M_2C decomposition pathway *via* a new dislocation-nucleation manner besides the common interface-nucleation mode. New precipitates are nucleated either along dislocations or at intersections of dislocations and stacking faults. It should be emphasized that the predominant decomposition pathway may evolve with decomposition time, temperature, and pre-strain. The interface-nucleation mode is more active in the initial decomposition stage, whereas the dislocation-nucleation manner may dominate the later decomposition process after the formation of thin product layers at the matrix/M_2C interface. An increase of temperature causes dislocation annihilation and enables an evolution of decomposition pathway from the dislocation-nucleation mode to the interface-nucleation one. Larger pre-strains produce higher dislocation densities in M_2C carbides and create more

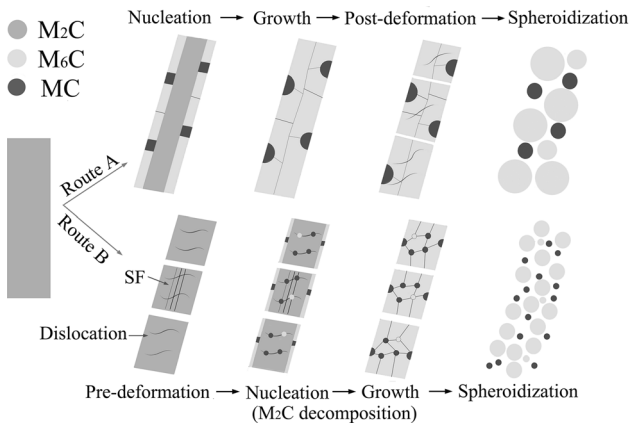

Fig. 18—Schematic description of M_2C carbide evolution for different processing routes. Routes A and B are herein referred to as the conventional route and the novel route developed in this work, respectively.

nano-precipitates in carbide interiors, evidencing the reinforced dislocation-nucleation mode with increasing strain.

D. *Role of Pre- and Post-deformation in Tuning Carbides*

Pre- and post-deformation relative to the carbide decomposition step may play different roles in tuning primary carbides of HSS, as schematically described in Figure 18. For the conventional processing route, the predominant role of post-compression lies in mechanical disruption and dispersion of decomposed carbide mixtures. Post-compression has no impact on carbide decomposition whereas may to some extent accelerate carbide spheroidization.

Pre-compression employed in this work can not only crush carbide networks into dispersive smaller fragments, but also accelerate carbide decomposition and spheroidization. Compression-induced defects in M_2C carbides, acting as potential nucleation sites, enhance significantly nucleation rates of new precipitates and produce precipitates with higher number densities and smaller dimensions. The following spheroidization treatment further disperses these carbide mixtures. Compared with post-compression, pre-compression enables much higher decomposition rates at a given temperature and produces smaller-sized carbides at a given strain. It can be inferred that lower temperatures and smaller strains are required to completely decompose and disperse carbides. This may offer an opportunity to overcome shortcomings of conventional processing route and an alternative pathway for carbide refinement of HSS.

V. SUMMARY

The present work employs a pre-compression step and investigates its effect on the following carbide decomposition and spheroidization in HSS. Several important conclusions are made and presented below.

(1) Pre-compression may introduce dislocations into M_2C carbides and hence significantly enhance M_2C decomposition. These structural defects can serve as potential nucleation sites of new precipitates and activate an alternative M_2C decomposition pathway *via* a new dislocation-nucleation mode besides the common interface-nucleation manner.

(2) The enhancement effect of pre-compression on M_2C decomposition exhibits a dependence on pre-strain and decomposition temperature, which originates from the temperature-mediated balance between dislocation densities and element diffusion. The optimal decomposition temperature in the present work is around 1050 °C probably due to a good combination of residual dislocation densities and element diffusion rates.

(3) Compared with post-compression, pre-compression significantly enhances precipitate nucleation rates and enables smaller-sized precipitates and higher tempered hardness. Pre-compression followed by carbide decomposition and spheroidization offers an alternative pathway of preparing HSS with a homogeneous microstructure.

ACKNOWLEDGMENTS

This work was supported financially by the National Natural Science Foundation of China (Project Nos. 51301038, 51371050, and 51201031).

REFERENCES

1. M. Boccalini and H. Goldenstein: *Int. Mater. Rev.*, 2001, vol. 46, pp. 92–115.
2. H. Fredriksson, M. Hillert, and M. Nica: *Scand. J. Metall.*, 1979, vol. 8, pp. 115–22.
3. F.S. Pan, W.Q. Wang, A.T. Wang, L.Z. Wu, T.T. Liu, and R.J. Cheng: *Prog. Nat. Sci.*, 2011, vol. 21, pp. 180–86.
4. E.S. Lee, W.J. Park, K.H. Baik, and S. Ahn: *Scr. Mater.*, 1998, vol. 39, pp. 1133–38.
5. Y. Tian, O.I. Gorbatov, A. Borgenstam, A.V. Ruban, and P. Hedstrom: *Metall. Mater. Trans. A*, 2017, vol. 48A, pp. 1–7.
6. S. Kasai, S. Ukai, T. Yamashiro, S. Zhang, N. Oono, S. Hayashi, S. Ohtsuka, and H. Sakasegawa: *Metall. Mater. Trans. A*, 2019, vol. 50A, pp. 590–600.
7. Z.H. Cai, H. Ding, R.D.K. Misra, and Z.Y. Ying: *Acta Mater.*, 2015, vol. 84, pp. 229–36.
8. X. Li, L.Q. Chen, Y. Zhao, X.Y. Yuan, and R.D.K. Misra: *Mater. Sci. Eng. A*, 2018, vol. 715, pp. 257–65.
9. K. Li, V.S.Y. Injeti, R.D.K. Misra, Z.H. Cai, and H. Ding: *Mater. Sci. Eng. A*, 2018, vol. 711, pp. 515–23.
10. M.H. Zhang, L.F. Li, J. Ding, Q.B. Wu, Y.D. Wang, J. Almer, F.M. Guo, and Y. Ren: *Acta Mater.*, 2017, vol. 141, pp. 294–303.
11. B. Avishan: *Mater. Sci. Eng. A*, 2018, vol. 729, pp. 362–69.
12. G.B. Olson and M. Cohen: *Metall. Trans. A*, 1975, vol. 6, pp. 791–95.
13. T. Iwamoto and T. Tsuta: *Int. J. Plasticity*, 2000, vol. 16, pp. 791–804.
14. R.G. Stringfellow, D.M. Parks, and G.B. Olson: *Acta Metall. Mater.*, 1992, vol. 40, pp. 1703–16.
15. H.C. Shin, T.K. Ha, and Y.W. Chang: *Scr. Mater.*, 2001, vol. 45, pp. 823–29.
16. X.F. Zhou, Z.X. Zheng, W.C. Zhang, F. Fang, Y.Y. Tu, and J.Q. Jiang: *Metall. Mater. Trans. A*, 2020, vol. 51A, pp. 568–73.
17. X.F. Zhou, D. Liu, W.L. Zhu, F. Fang, Y.Y. Tu, and J.Q. Jiang: *J. Iron Steel Res. Int.*, 2017, vol. 24, pp. 43–49.
18. E.S. Lee, W.J. Park, J.Y. Jung, and S. Ahn: *Metall. Mater. Trans. A*, 1998, vol. 29A, pp. 1395–1404.
19. X.F. Zhou, F. Fang, J.Q. Jiang, W.L. Zhu, and H.X. Xu: *Mater. Sci. Technol.*, 2012, vol. 28, pp. 1499–1504.
20. W.S. Williams: *J. Appl. Phys.*, 1964, vol. 35, pp. 1329–38.
21. N.D. Leon, B. Wang, C.R. Weinberger, L.E. Matson, and G.B. Thompson: *Acta Mater.*, 2013, vol. 61, pp. 3905–13.
22. J.D. Bolton and M. Redington: *J. Mater. Sci.*, 1980, vol. 15, pp. 3150–56.
23. N. Cautaerts, R. Delville, E. Stergar, D. Schryvers, and M. Verwerft: *Acta Mater.*, 2019, vol. 164, pp. 90–98.
24. Z.Q. Feng, Y.Q. Yang, B. Huang, X. Luo, M.H. Li, M. Han, and M.S. Fu: *Acta Mater.*, 2011, vol. 59, pp. 2412–22.
25. J. Takahashi, K. Kawakami, J. Hamada, and K. Kimura: *Acta Mater.*, 2016, vol. 107, pp. 415–22.
26. N.C. Eurich and P.D. Bristowe: *Scr. Mater.*, 2015, vol. 102, pp. 87–90.